PNAS RESEARCH ARTICLE | IMMUNOLOGY AND INFLAMMATION

Adipose-tissue regulatory T cells are a consortium of subtypes that evolves with age and diet

Andrés R. Muñoz-Rojas[a], Gang Wang[a], Christophe Benoist[a], and Diane Mathis[a,1]

Contributed by Diane Mathis; received November 22, 2023; accepted December 8, 2023; reviewed by Marco Colonna and Jeffrey V. Ravetch

Foxp3$^+$CD4$^+$ regulatory T (Treg) cells found within tissues regulate local immunity, inflammation, and homeostasis. Tregs in epididymal visceral adipose tissue (eVAT) are critical regulators of local and systemic inflammation and metabolism. During aging and under obesogenic conditions, eVAT Tregs undergo transcriptional and phenotypic changes and are important for containing inflammation and normalizing metabolic indices. We have employed single-cell RNA sequencing, single-cell *Tra* and *Trb* sequencing, adoptive transfers, photoconvertible mice, cellular interaction analyses, and in vitro cultures to dissect the evolving heterogeneity of eVAT Tregs with aging and obesity. Distinct Treg subtypes with distinguishable gene expression profiles and functional roles were enriched at differing ages and with differing diets. Like those in lean mice, eVAT Tregs in obese mice were not primarily recruited from the circulation but instead underwent local expansion and had a distinct and diversified T cell receptor repertoire. The different eVAT-Treg subtypes were specialized in different functions; for example, the subtypes enriched in lean, but not obese, mice suppressed adipogenesis. The existence of functionally divergent eVAT-Treg subtypes in response to obesogenic conditions presents possibilities for precision therapeutics in the context of obesity.

regulatory T cells | adipose tissue | obesity | single-cell | T cell receptor

Regulatory T cells (Tregs) are important regulators of immune responses. Early studies focused on the ability of circulating Tregs to reign in excessive autoimmunity and inflammation; however, recent work has established the importance of tissue-localized Tregs in regulating not only local immune responses but also tissue physiology. These so-called "tissue-Tregs" have distinct transcriptional profiles, cytokine and growth factor dependencies, and T cell receptor (TCR) repertoires that allow them to operate optimally in distinct tissue environments (1).

Tregs within epididymal (e) visceral adipose tissue (VAT) were the first tissue-Treg compartment to be characterized (2). eVAT Tregs accumulate with age, eventually making up the majority of eVAT CD4$^+$ T cells in lean adult mice, wherein they regulate tissue immune and inflammatory responses as well as local and systemic metabolism. eVAT Tregs express a specific set of transcription factors and cytokine receptors, such as PPARγ and the interleukin (IL)-33 receptor, ST2, as well as distinct TCR repertoires, which together promote their accumulation, survival, and function in adipose tissue (3–8). eVAT Tregs interact with diverse cell populations in the neighborhood, including VAT mesenchymal stromal cells (VmSCs), macrophages (MFs), and adipocytes. Cross talk with VmSCs directly regulates eVAT-Treg accumulation—for example, via IL-33 (9). MFs are similarly required for eVAT-Treg accumulation (10), and, in turn, eVAT Tregs regulate inflammatory MFs to limit local inflammation (2, 10). In obesogenic conditions, eVAT Tregs regulate both local and systemic inflammation and metabolic indices (2, 3, 5, 7, 11–15). Tregs improve insulin sensitivity in part by regulating obesity-induced inflammation, and the striking loss of eVAT Tregs in obese mice further exacerbates inflammation and the worsening of metabolic indices (13). Furthermore, the characteristic eVAT-Treg transcriptional profile is lost in obese mice, suggesting a defective, or at least distinct, functional capacity (16).

Despite the growing body of evidence on the importance and function of eVAT Tregs, most of their characterizations have been performed at the population level. As a wealth of recent studies have demonstrated, many tissue-localized cell types display extensive heterogeneity, important for maximizing their functional options. Recent studies have leveraged single-cell technologies to dissect heterogeneity in eVAT as a whole or in subcutaneous adipose tissue and eVAT Tregs from lean mice (14, 17, 18). However, we still do not know whether and how the heterogeneity of eVAT Tregs changes with age and during obesity and whether particular eVAT-Treg subtypes have distinct ontogenies, TCR repertoires, interaction partners, or functional roles. We used a combination of experimental and computational approaches to address this knowledge gap. Aging and obesity promoted the accumulation of distinct eVAT-Treg subtypes, with different TCR

Significance

Regulatory T cells (Tregs) have emerged as promising candidates for modulating the immunological control of tissue physiology. The Tregs found in epididymal visceral adipose tissue (eVAT) are important regulators of local and systemic metabolism in obesogenic conditions, both by containing inflammation and by normalizing metabolic parameters. Do distinct eVAT-Treg subtypes regulate various physiological parameters? We used a combination of computational and experimental analyses to show that multiple functional Treg subtypes exist in eVAT, that their distribution evolves with aging and diet, and that they have divergent predicted specificities for their T cell receptors. Targeting specific eVAT-Treg subtypes suggests potential therapeutic approaches for precision medicine in the obesity field.

Author affiliations: [a]Department of Immunology, Harvard Medical School, Boston, MA 02115

Author contributions: A.R.M.-R. and D.M. designed research; A.R.M.-R. and G.W. performed research; A.R.M.-R. and G.W. analyzed data; C.B. and D.M. supervised; and A.R.M.-R. and D.M. wrote the paper.

Reviewers: M.C., Washington University in St. Louis School of Medicine; and J.V.R., The Rockefeller University.

Competing interest statement: C.B., D.M., and Marco Colonna are members of the ImmGen Consortium, a grand endeavor devoted to immunocyte genomics, and have appeared as co-authors in this context.

Copyright © 2024 the Author(s). Published by PNAS. This article is distributed under Creative Commons Attribution-NonCommercial-NoDerivatives License 4.0 (CC BY-NC-ND).

[1]To whom correspondence may be addressed. Email: dm@hms.harvard.edu.

This article contains supporting information online at https://www.pnas.org/lookup/suppl/doi:10.1073/pnas.2320602121/-/DCSupplemental.

Published January 16, 2024.

Downloaded from https://www.pnas.org by HARVARD UNIVERSITY CABOT SCIENCE LIBRARY on February 2, 2024 from IP address 128.103.147.149.

repertoires and functional capacities vis-à-vis those of eVAT Tregs in lean adult mice.

Results

Heterogeneity of eVAT Cell Populations with Aging and Obesity. eVAT undergoes profound cellular and transcriptional alterations during aging and with obesity. eVAT Tregs accumulate with age in lean mice and decrease when obesity sets in, accompanied by large transcriptional changes. Outstanding questions are whether and how the cellular niche around eVAT Tregs evolves in parallel, and how these changes affect eVAT-Treg abundance, phenotype, and function. To address these questions, we performed single-cell RNA sequencing (scRNA-seq) on both the whole stromal vascular fraction (SVF) and sorted eVAT Tregs from mice fed either low-fat diet (13% kcal fat) (LFD) or high-fat diet (60% kcal fat) (HFD) for 16 wk, starting at 14 wk of age. As expected, mice fed a HFD for 16 wk showed a large body weight increase while those maintained on a LFD did not (*SI Appendix*, Fig. S1*A*). To deconvolute the effects of aging and diet, we included cells from LFD-fed, 14-wk-old mice as well (Fig. 1*A*). We also performed population-level RNA-seq on floated adipocytes from each of the three mouse groups to assess transcriptional changes in the local parenchymal cell compartment. After doublet removal, quality filtering, and integration of two independent experiments, we generated a cellular map consisting of 16,427 SVF cells and 5,062 eVAT Tregs (Fig. 1*B* and *SI Appendix*, Fig. S1*B*). Using a combination of annotation algorithms and manual curation, we identified multiple immunocyte, stromal cell, and endothelial cell populations, delineated by their characteristic marker transcripts (Fig. 1*C*).

Population sizes and transcriptomes in eVAT from mice maintained on LFD were generally quite similar across the ages examined (Fig. 1 *D*–*F*). Even though there were some small changes in cellular compositions between mice of different ages on LFD, most cell types occupied the same two-dimensional space in the Uniform Manifold Approximation and Projection (UMAP) representation, suggesting similar global transcriptional profiles (Fig. 1*D*). To better quantify the transcriptional similarity between eVAT cells from mice of different ages and on different diets, we performed partition-based graph abstraction (PAGA) analysis. PAGA uses a statistical model to evaluate how connected two groups are against what is expected at random (19). This approach quantifies similarity using the high-dimensionality neighborhood graph representation of single-cell data and thus avoids the distortions and loss of information inherent in two-dimensional representations. Using this method, we observed that most cell types from lean mice of the two ages had high similarity scores (Fig. 1*E*).

Under obesogenic conditions, the changes in cellular composition and transcriptional profiles were larger (Fig. 1 *D*–*F*). There was a proportional augmentation of VmSCs, $CD8^+$ T cells, mast cells (MCs), and MFs and a loss of ILC2s, natural killer (NK) cells, and ECs (Fig. 1*F*). Some cell types, in particular VmSCs and MFs, acquired a distinct transcriptional profile in obese mice (Fig. 1*E*). The dramatic increase in MFs upon HFD feeding previously reported was not observed, likely reflecting differences in the precise feeding protocols employed (17, 20). We aged the mice to 14 wk before placing them on HFD to enable expansion of the Treg compartment before HFD feeding and to better model adult-onset obesity. In contrast, VmSCs showed a large proportional increase in obese mice, accompanied by profound transcriptional changes (Fig. 1 *E* and *F*).

This cellular map provides a useful resource for studying the cellular and transcriptional heterogeneity of murine eVAT with aging and obesity. Below we demonstrate its utility for studying cell:cell interactions, for example.

eVAT-Treg Heterogeneity. To assess the heterogeneity of eVAT Tregs and how it might evolve with aging or obesity, we distilled out the eVAT-Treg scRNA dataset and performed dimensionality reduction and clustering. There were seven distinct subtypes, which we named Early Activation, *Areg*^{lo}*Il1rl1*$^+$, *Areg*^{hi}*Il1rl1*$^+$, *Tbx21*$^+$, *Il18r1*$^+$, ISG$^+$, and Quiescent (Fig. 2*A*). The parsing and naming of clusters were validated by visualizing the most differentially expressed genes (Fig. 2*B* and *SI Appendix*, Fig. S2*A*), and recapitulated the previously reported eVAT-Treg subtypes of lean mice (18). Two *Il1rl1*$^+$ subtypes showed high expression of their eponymous transcript, which encodes ST2, the IL-33 receptor. The *Areg*^{hi} subtype was distinguishable from the *Areg*^{lo} subtype by its high expression of, for example, *Areg*, *Nr4a1*, *Junb*, *Fosb*, *Nfkbia*, *Nfkbid,* and *Nfkbiz* (Fig. 2*B* and *SI Appendix*, Fig. S2*B*), and the relative abundance of these two clusters is known to be circadian-rhythm dependent (18). The *Tbx21*$^+$ subtype had enriched expression of, for example, *Cxcr3*, *Cd74,* and *Tbx21*, while the *Il18r1*$^+$ subtype had higher levels of *Il18r1*, *Itgb1*, *Cxcr3*, *Pycard,* and *S1pr1*. The Quiescent subtype expressed elevated levels of, for e.g., *S1pr1*, *Sell,* and *Tcf7*, typically enriched in naive T cells (21), while the Early Activation subtype expressed enriched levels of *Nme1*, *Tnfrsf9,* and *Mif.* The ISG subtype was a small one that expressed several interferon-response gene transcripts, such as *Isg15*, *Stat1,* and *Ifit1* (Fig. 2*B* and *SI Appendix*, Fig. S2*A*).

To evaluate the effect of mouse physiology on the representation of these clusters, we projected the data from mice of the individual age and diet groups onto the UMAP plot used to visualize the totality of eVAT Tregs and quantified the proportional membership of each cell cluster for each mouse group (Fig. 2*C*). There were pronounced alterations in the subtype distributions with differences in both age and diet. As reported previously (18), both *Il1rl1*$^+$ subtypes were highly represented in lean mice, and their enrichment increased with age (compare the blue and orange data). In mice fed a HFD, both *Il1rl1*$^+$ subtypes showed a dramatic decrease in proportion, disappearing almost entirely from the eVAT-Treg compartment (compare the orange and green data). On the other hand, the *Tbx21*$^+$ subtype constituted a smaller fraction of the eVAT-Treg compartment in both young and older lean mice but showed a pronounced proportional increase with HFD feeding. Both the Quiescent and *Il18r1*$^+$ subtypes proportionally decreased with age, but were maintained or even slightly increased in mice fed a HFD (Fig. 2*C*). The Early Activation and ISG subtypes were the smallest clusters and did not show large alterations with age or diet. Thus, young lean mice hosted the greatest variety of eVAT-Treg subtypes; as the mice aged, the eVAT-Treg compartment became more specialized, with enrichment of either the *Il1rl1*$^+$ or *Tbx21*$^+$ subtypes, depending on the diet. Previous population-level RNAseq analyses showed that eVAT Tregs die and lose their characteristic transcriptional profile in obese mice, including loss of the transcript encoding their defining transcription factor, PPARγ (3, 13, 16). The current single-cell analysis provides more precision to these observations, establishing that long-term HFD drove the enrichment of a distinct subtype of eVAT Tregs with low expression of *Pparg* and high expression of *Tbx21* (*SI Appendix*, Fig. S2*C*), suggesting that the eVAT-Treg subtypes in obese mice might have transcriptional dependencies that differ from those of lean mice.

We then asked how the various eVAT-Treg subtypes were related to each other and whether their distinct transcriptional states might represent distinct differentiation trajectories acquired in the tissue. Hence, we performed RNA-velocity analysis, which

Downloaded from https://www.pnas.org by HARVARD UNIVERSITY CABOT SCIENCE LIBRARY on February 2, 2024 from IP address 128.103.147.149.

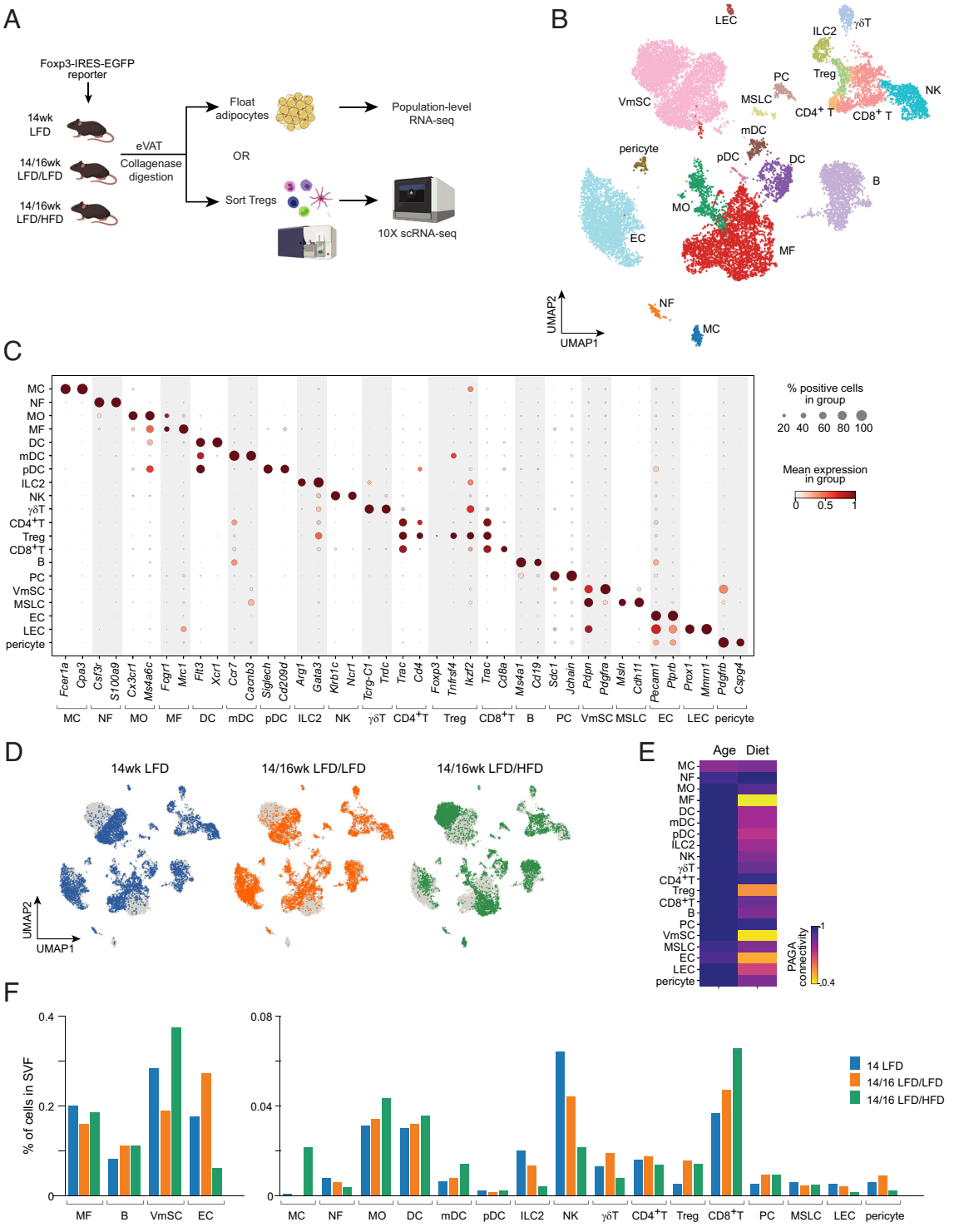

Fig. 1. Single-cell map of the SVF of eVAT with aging and obesity. (*A*) Experimental schema. scRNA-seq analysis of 14-wk-old *Foxp3-Gfp* mice placed on a LFD or HFD for 16 wk. (*B*) UMAP representation of the scRNA-seq data from the combined SVFs with the identified cell types. (*C*) Expression of cell-type marker genes by each identified population. (*D*) Overlay of the UMAP representation of the eVAT SVF from the individual mouse groups on the total eVAT SVF data. (*E*) Heatmap of the PAGA connectivity measures for each cell population across the different ages and diets. (*F*) Proportional representation of each cell population within each mouse group. Combined data from two independent experiments. LFD, low-fat diet; HFD, high-fat diet; eVAT, epididymal visceral adipose tissue; UMAP, Uniform Manifold Approximation and Projection; MC, mast cells; NF, neutrophils; MO, monocytes; MF, macrophages; DC, dendritic cells; mDC, migratory dendritic cells; pDC, plasmacytoid dendritic cells; ILC2, type 2 innate lymphoid cells; NK, natural killer cells; γδT, γδ T cells; CD4$^+$T, CD4$^+$ T cells; Treg, regulatory T cells; CD8$^+$T, CD8$^+$ T cells; B, B cells; PC, plasma cells; VmSC, VAT mesenchymal stromal cells; MSLC, mesothelial cells; EC, endothelial cells; LEC, lymphatic endothelial cells; PAGA, partition-based graph abstraction.

uses the ratio of spliced to unspliced transcripts to quantify newly produced transcripts and predict the future transcriptional state of each cell (22, 23). RNA-velocity revealed trajectories differing between the various eVAT-Treg subtypes with high confidence (Fig. 2*D*). One trajectory started in the Early Activation cluster and moved toward the *Areg*^{lo}*Il1rl1*$^+$ and *Areg*^{hi}*Il1rl1*$^+$ clusters. Other trajectories also started in the Early Activation cluster but moved directly into the *Tbx21*$^+$ cluster or to the Quiescent cluster

Downloaded from https://www.pnas.org by HARVARD UNIVERSITY CABOT SCIENCE LIBRARY on February 2, 2024 from IP address 128.103.147.149.

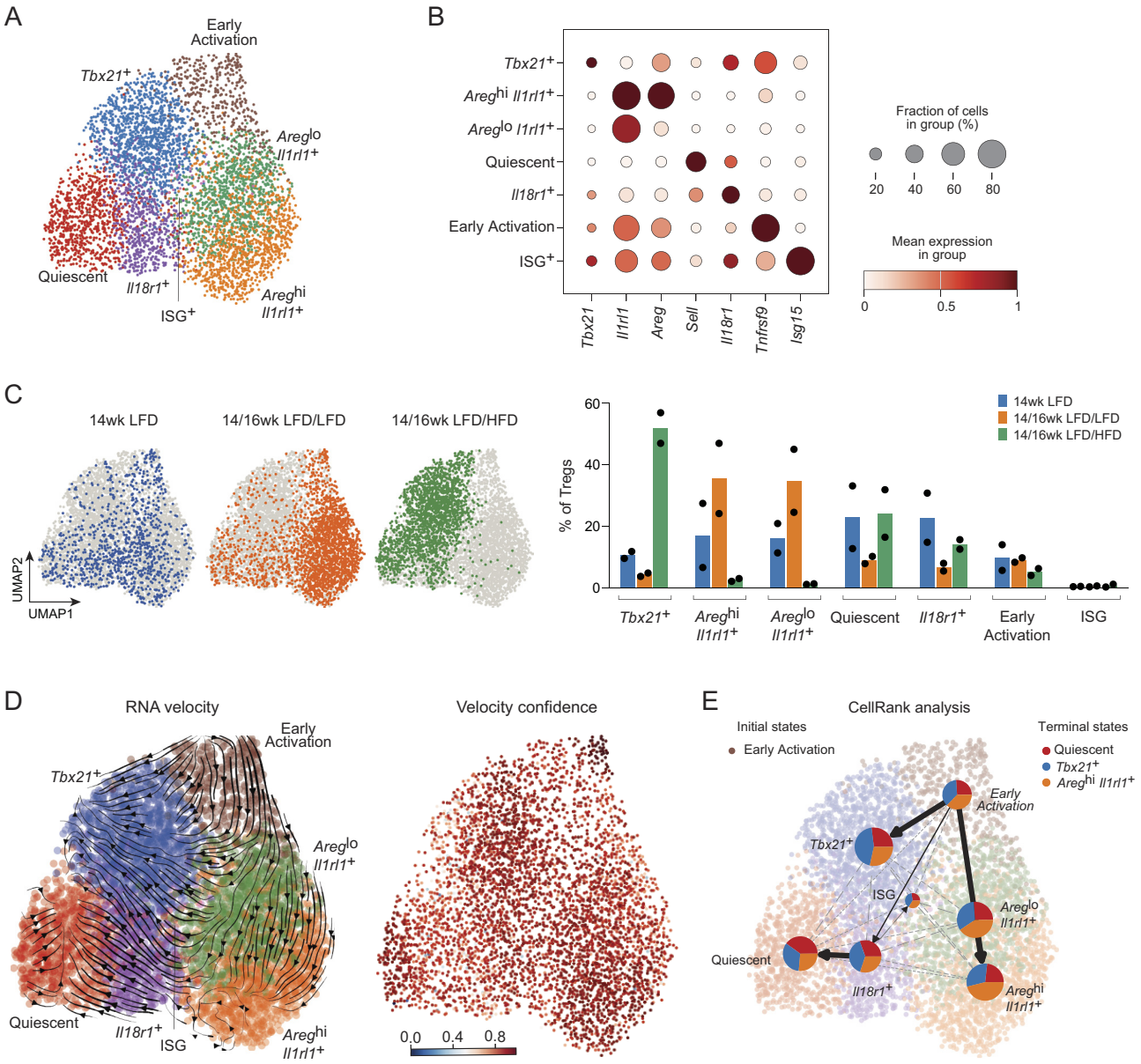

Fig. 2. Phenotype and provenance of eVAT-Treg subtypes. (*A*) UMAP representation of the eVAT-Treg subtypes (n = 2). (*B*) Expression of genes delineating the various eVAT-Treg subtypes. (*C*) Overlap of the eVAT-Treg data for the various groups on the total eVAT-Treg data (*Left*), and quantification of their proportional abundances in each group's total eVAT Tregs (*Right*). (*D*) RNA-velocity analysis of eVAT-Treg subtypes. Velocity vectors (*Left*) and velocity confidence (*Right*) overlain on the UMAP representation. (*E*) CellRank analysis of the eVAT-Treg clusters depicting the initial, terminal, and predicted differentiation paths. Trajectories are represented as an overlain partition-based abstraction graph. Pie charts depict the absorption probability states toward terminal states averaged within that cluster. The edges show the direction of the inferred trajectory, and the thickness represents the transcriptional similarity between clusters. Combined data from two independent experiments. ISG, interferon-stimulated genes; other abbreviations as per Fig. 1.

via the *Il18r1*$^{+}$ cluster. To more robustly quantify these RNA-velocity trajectories, we used CellRank, which combines trajectory inference with RNA velocity to predict initial and terminal macrostates, infer fate probabilities and estimate the differentiation direction of cell states (24). CellRank analysis predicted that Early Activation was an initial state, while the Quiescent, *Tbx21*$^{+}$, and *Areg*^{hi}*Il1rl1*$^{+}$ clusters were predicted to be terminal states (Fig. 2*E*). Thus, the Early Activation cluster split into three distinct trajectories: one progressing toward the *Areg*^{hi}*Il1rl1*$^{+}$ cluster, passing through the *Areg*^{lo}*Il1rl1*$^{+}$ cluster; another toward the *Il18r1*$^{+}$ cluster, ending in the Quiescent cluster, and one straight into the *Tbx21*$^{+}$ cluster. These analyses suggested that cells of the Early Activation subtype were the earliest Tregs to arrive in the tissue, serving as a seed population of cells that differentiated into mature *Il1rl1*$^{+}$, *Tbx21*$^{+}$, and Quiescent Tregs, depending on the tissue microenvironment molded by the age and diet of the mice.

The eVAT-Treg TCR Repertoire Changes with Obesity. Next, we explored how the repertoire of TCRs displayed on eVAT Tregs changed with obesity. We placed 14-wk-old *Foxp3*$^{Thy1.1}$ mice on either a LFD (lean) or HFD (obese) for 16 to 24 wk and performed paired scRNA-seq and single-cell sequencing of both the alpha and beta chains (sc*Tra/b*-seq) on Tregs sorted from their eVAT depot and spleen. For the most part, eVAT Tregs clustered separately from splenic Tregs in 2D UMAP space, although there was minor incursion of eVAT Tregs into the splenic Treg space in both lean and obese mice. The eVAT Tregs from lean vs. obese mice also clustered largely separately, again pointing to distinct

Downloaded from https://www.pnas.org by HARVARD UNIVERSITY CABOT SCIENCE LIBRARY on February 2, 2024 from IP address 128.103.147.149.

transcriptional states across diets (Fig. 3*A*). In contrast, the splenic Tregs from mice on the two diets did not show changes in their UMAP distribution. To determine whether the transcriptional drift seen in eVAT Tregs from obese mice reflected a phenotype more similar to that of their splenic counterparts, we calculated a gene expression score from the most differentially expressed genes of mice on the two diets. By definition, the "Obese eVAT Treg Signature" was highly expressed in eVAT from obese (but not lean) mice, but also in splenic Tregs of both groups, indicating that these three populations shared a similar transcriptional state (Fig. 3*B*). For a more global view, we performed PAGA analysis to quantify the connectivity and similarity between the various Treg populations in high-dimensional transcriptional space. The resulting plot revealed Tregs from the same tissue to have the highest transcriptional similarity (thicker lines), while eVAT Tregs from obese, but not lean, mice showed cross-tissue similarity to the two splenic Treg populations (Fig. 3*C*).

Because of extreme diversity in the nucleotide sequences of TCRs on T cells, each one's sequence can be useful as a natural barcode to indicate clonally related cells with divergent phenotypes, reflecting either a precursor:product relationship or emergence from a common precursor. Using this *Tra/b*-barcoding technique, we previously reported that the eVAT Treg compartment is seeded early in life and undergoes large local expansions in lean mice (2, 4), but what happens to such clonally expanded cells in obese mice remained unknown. In the current study as well, lean mice harbored highly expanded clonal populations of eVAT Tregs and low diversity of *Tra/b* sequences, with some mice having over 80% repeated *Tra/b* sequences of which a single clone accounted for almost 50% of the entire Treg compartment (Fig. 3 *C* and *D* and *SI Appendix*, Fig. S3 *B* and *C*). (Note: We defined clonally related cells as those having exactly the same *Tra* and *Trb* nucleotide sequences). Obese mice had strikingly fewer clonal expansions (around 35%), closer to but still higher than the clonality observed in splenic Tregs. Obese eVAT Tregs also had no major dominant clone in any mouse (Fig. 3 *C* and *D*). Splenic Tregs had more clonal expansions than previously reported, likely due to the advanced age of the mice profiled.

We then asked whether there were any clonal relationships between the various eVAT Treg subtypes identified above. Reclustering the eVAT Tregs from the 7 mice examined recapitulated the eVAT-Treg subtypes detailed in Fig. 2 and *SI Appendix*, Fig. S2 (*SI Appendix*, Fig. S3*E*). The most clonally related subtypes, which also contained some of the largest clones, were the two *Il1rl1*$^+$ subtypes, consistent with the observation that they were also transcriptionally the most similar (Fig. 3*F*). The two *Il1rl1*$^+$ subtypes also shared five clones with the *Tbx21*$^+$ subtype, certain of which were substantially expanded, indicating that eVAT Tregs sharing a common ancestor can adopt distinct subtypes. The Early Activation subtype shared clones with all other subtypes, including some that were shared across multiple subtypes and had notable clonal expansions (~10 cells) (Fig. 3*F*), reminiscent of the RNA-velocity analysis in suggesting that the Early Activation subtype is a putative seed population engendering other eVAT-Treg subtypes.

Were any eVAT-Treg TCRs shared across mice? All the eVAT Treg clones, defined as such by having identical *Tra* and *Trb* nucleotide sequences, were found only within the same mouse (Fig. 3*G*). However, we did pick up four clones with identical TCR amino acid sequences but different nucleotide sequences, suggestive of selection pressure to recognize a particular antigen. These clones were always shared between mice on the same diet—never those on different diets—suggesting that some eVAT Tregs recognized the same antigen, one that was distinct between eVAT of lean vs. obese mice (Fig. 3*H*). Since TCRs with different amino acid sequences can still recognize the same antigen, we also applied a TCR-clustering algorithm that allows for some amino acid substitutions based on their chemical properties and then clusters the TCRs based on similarity. There were larger clusters of TCRs with similar amino acid sequences, including some that contained highly expanded clones (Fig. 3*I*). TCRs with similar amino acid sequences were shared only between mice on the same diet, further suggesting a shared specificity in eVAT-Treg TCRs that differs between lean and obese mice. Similar results were obtained with an even more permissive algorithm (GLIPH2), which clusters TCRs based on amino acid motifs (25) (*SI Appendix*, Fig. S3*D*).

In aggregate, the TCR analysis revealed distinct TCR clonalities and repertoires in eVAT Tregs of lean and obese mice and suggested that distinct antigens might be recognized in the two nutritional states. Interestingly, eVAT-Treg subtypes can share ancestry across different subtypes.

eVAT Tregs in Obese Mice Expand Locally, with Only a Minor Contribution from Circulating Tregs. The eVAT-Treg compartment in lean adult mice is seeded early in life, contains little contribution from circulating Tregs, and is greatly diminished with obesity (2, 4, 13). The source of the residual eVAT-Treg compartment in obese mice is currently unknown. It is possible that a death-resistant component of the eVAT-Treg population expanded, that the obese state promoted recruitment from the circulating Treg pool, or some combination of the two. We took multiple approaches to distinguish between these possibilities. Initially, we exploited the *Tra/b*-barcoding technique to quantify sharing of clones between eVAT and splenic Tregs in mice on the two diets. We used the Jaccard index to quantify the cross-tissue repertoire similarity and normalize across different compartment sizes. Some of the obese mice had a higher Jaccard index but, overall, the difference between the two groups was not statistically significant (P = 0.224) (Fig. 4*A*). The level of N-nucleotide addition in the *Trb*, but not the subsequently rearranged *Tra* gene, was similarly reduced in the expanded eVAT-Treg clones from lean and obese mice in comparison with that of the expanded splenic Treg clones (Fig. 4*B*). [A similar but smaller difference was observed when comparing all, including nonexpanded, clones (*SI Appendix*, Fig. S4*A*)]. This finding suggests that the eVAT Tregs from both lean and obese mice differentiated around the time that terminal deoxynucleotidyl transferase (TdT) was turned on during the first week of life (26) and that the eVAT Tregs expanding in obese mice were also generated at that time and were not replaced by more recently generated Tregs from the circulation.

However, the TCR analysis might show an incomplete picture due to inadequate coverage of Treg clonality. Therefore, we took two other orthogonal approaches to quantify the contribution of Tregs from the circulation to eVAT of lean vs. obese mice. First, we performed an adoptive-transfer experiment using congenic mice to track Tregs introduced into the circulation. 14-wk-old CD45.1$^-$2$^+$ recipient mice were placed on a LFD or HFD for 4 wk, sorted splenic CD45.1$^+$2$^-$CD4$^+$ T cells were transferred into those mice, and the recipients were analyzed 6 to 10 wk later (schematized in Fig. 4*C*). There was no difference in the proportion or number of donor-derived Tregs in the eVAT of lean and obese mice, indicating no increase in recruitment from the circulation (Fig. 4 *D* and *E*). Second, we studied cell trafficking in Kaede mice, which express a photoconvertible reporter in all cells, allowing for noninvasive labeling and monitoring of cells emanating from the lymphoid organs (27). Kaede mice were placed on a LFD or HFD for 4 wk, transcutaneous photoconversion of the cervical lymph nodes (CLNs) was performed, and the CLNs,

Downloaded from https://www.pnas.org by HARVARD UNIVERSITY CABOT SCIENCE LIBRARY on February 2, 2024 from IP address 128.103.147.149.

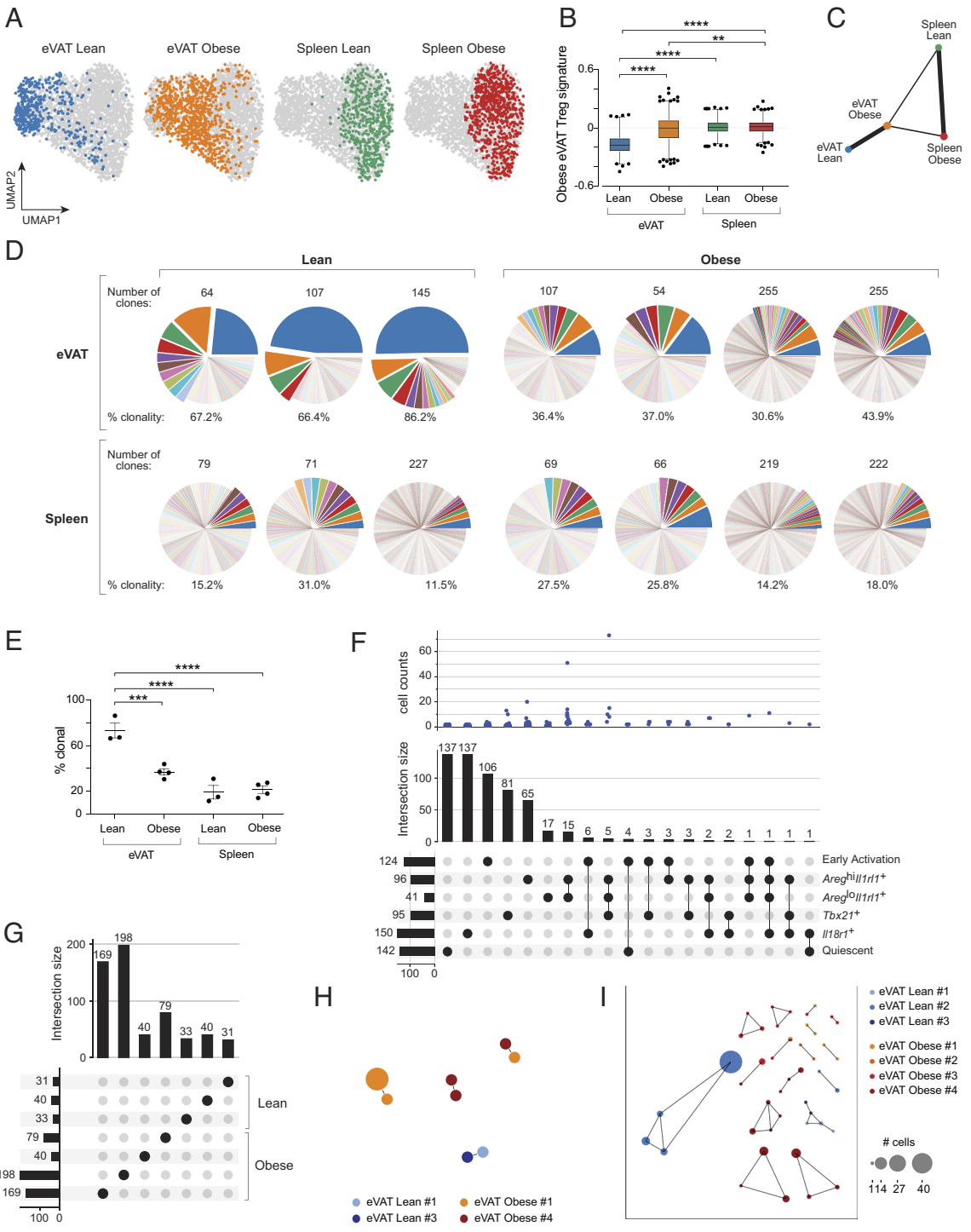

Fig. 3. Distinct TCR landscapes for eVAT Tregs of obese vs. lean mice. (*A*) eVAT and spleen scRNA-seq data from the individual groups overlain on the total dataset. (*B*) Boxplot of obese eVAT-Treg signature values, calculated as the gene expression score of the 50 most differentially expressed genes in eVAT Tregs from obese vs. lean mice. Box plots indicate the median and interquartile range (IQR). Values outside the range of the whiskers (1.5*IQR) are plotted as dots. Kruskal–Wallis test with Dunn's multiple comparison test; $^{**}P \leq 0.01$ and $^{****}P \leq 0.0001$. (*C*) PAGA graph comparing the gene expression profiles of Tregs from the various groups. (*D*) Pie charts of the sc*Tra/b*-seq data, depicting clonal expansions. For each mouse and tissue, clones were identified as groups of cells sharing the exact same CDR3 sequence in both *Tra* and *Trb*. The width of each slice represents the cell number in that clone. Note that shared colors do not represent shared clones. (*E*) Proportion of clonal cells, or cells with more than one shared clone, across tissues. Mean ± SEM, ordinary one-way ANOVA with Tukey's multiple comparison test; $^{***}P \leq 0.001$ and $^{****}P \leq 0.0001$. (*F* and *G*) Upset plot depicting the clonal overlap between the various eVAT-Treg clusters (*F*) or individual mice (*G*). The dot matrix (*Bottom*) specifies the compartments being compared, indicated as joined dots. The horizontal bar plot to the left of the dot matrix shows the number of individual clones for each subtype (*F*) or mouse (*G*). The bar plot (*Middle*) indicates the number of overlapping sequences for that comparison. The dot plot (*Top*) specifies the number of cells for each shared clone in that comparison. (*H* and *I*) Network visualization of TCR clones that have convergent protein sequences (*H*) or are predicted to have similar protein sequences (*I*). Each dot represents a unique *Tra/b* nucleotide sequence that is connected with other dots that share the exact same (*H*) or an identified similar (*I*) amino acid sequence. The size of the dots represents the number of cells with the same nucleotide sequence. Combined data from two independent experiments. Abbreviations as per Fig. 1.

Downloaded from https://www.pnas.org by HARVARD UNIVERSITY CABOT SCIENCE LIBRARY on February 2, 2024 from IP address 128.103.147.149.

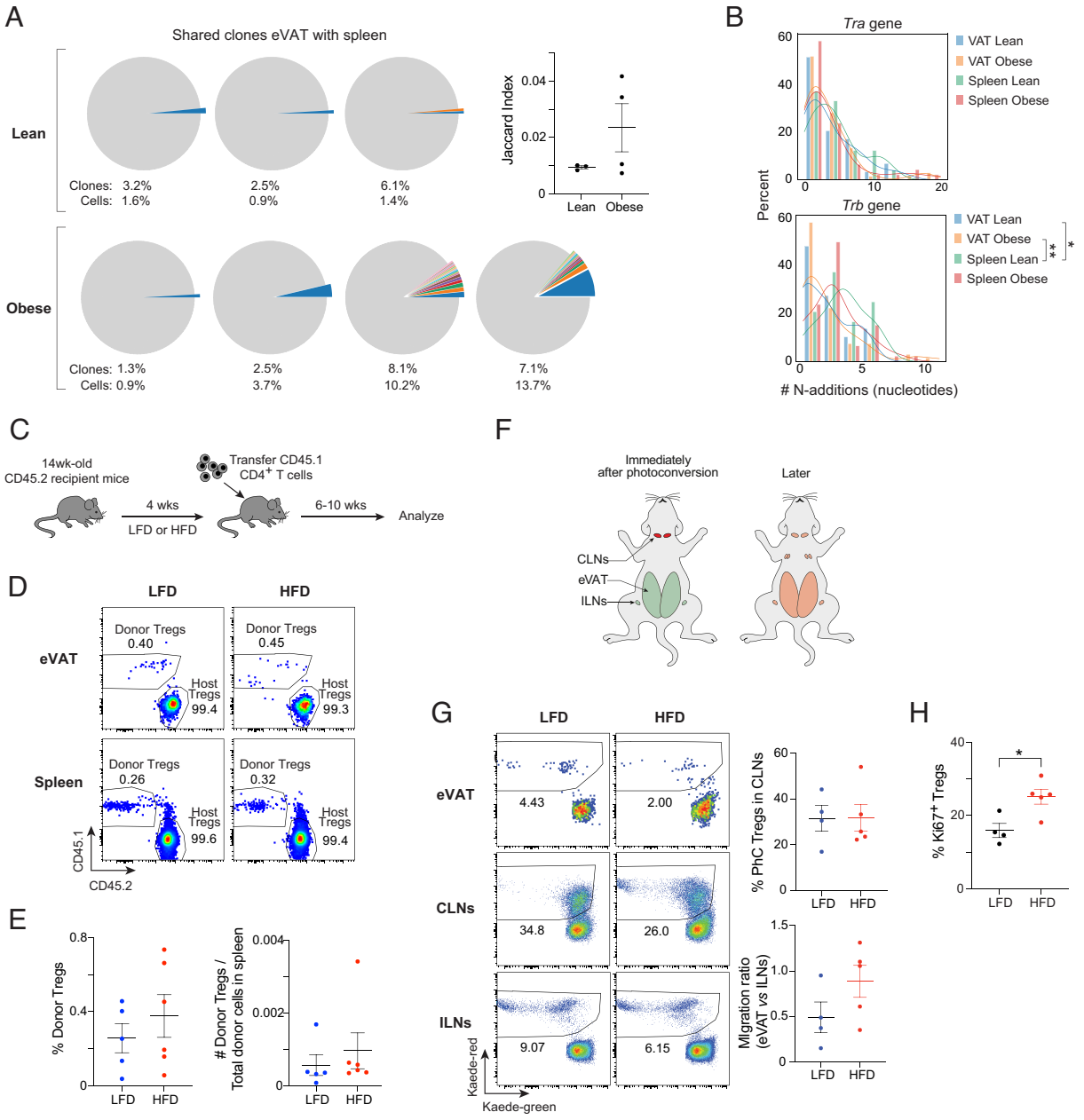

Fig. 4. Little recruitment, rather local proliferation, of eVAT Tregs in obese mice. (*A*) Pie charts (*Left*) depicting clones shared between eVAT and spleen Tregs. Colored slices indicate shared clones; the grayed-out portion represents nonshared clones. The similarity between the TCR repertoires of eVAT and spleen Tregs in each mouse was assessed by calculating the Jaccard index (*Right*). (*B*) Lengths of N-nucleotide additions. Significance values on the right via Kruskal–Wallis test with Dunn's multiple comparison test; $*P \leq 0.05$ and $**P \leq 0.01$. (*C*) Schema of adoptive transfer experiments. (*D*) Flow cytometry dot plots of donor- and host-derived Tregs in eVAT and spleen after transfer. (*E*) Quantification of the proportion (*Left*) and normalized number (*Right*) of donor-derived eVAT Tregs. Mean ± SEM, unpaired *t* test; $*P \leq 0.05$. N = 2 independent experiments. (*F*) Schematic of Kaede photoconversion experiments. (*G*) Flow cytometry dot plots (*Left*) and quantification (*Right*) of photoconverted Tregs in the eVAT, CLNs, and ILNs of mice 24 h postphotoconversion. (*H*) Flow cytometric quantification Ki67$^+$ cells, representing cells in cycle. Mean ± SEM, unpaired *t* test; $*P \leq 0.05$. N = 2 independent experiments.

inguinal lymph nodes (ILNs), and eVAT were analyzed 24 h later (schematized in Fig. 4*F*). There was no significant difference in the fraction of photoconverted Tregs remaining in the CLNs at that time point, indicating that obesity did not promote emigration from that site ($P = 0.967$) (Fig. 4*G*). Nor was there a significant difference in the propensity of CLN-derived Tregs from the two mouse groups to migrate to eVAT (normalized to the ILNs) ($P = 0.157$) (Fig. 4*G*), confirming that obesity did not render eVAT more "welcoming" to circulating Tregs. There was an increase in proliferation of eVAT Tregs in obese mice, quantified by Ki67 expression (Fig. 4*H*). Together, these results suggest that eVAT Tregs in obese mice have minimal contributions from circulation and instead undergo local expansion during obesity.

***Tbx21*$^+$ eVAT Tregs in Obese Mice Lose Their Ability to Inhibit Adipogenesis.** Finally, we compared the ability of the various eVAT-Treg subtypes to regulate adipose-tissue biology. As a hypothesis-generating tool, we used cell:cell communication analysis to explore putative interaction partners and signaling pathways used by eVAT Tregs, in particular how they were potentially modulated with obesity. The recently developed MultiNicheNet program (28), which enables cross-condition comparisons and incorporates the intracellular signaling downstream of a ligand-receptor pair to enrich for interactions that are not only expressed but also most likely to be operating. eVAT Tregs displayed enriched potential interactions with VmSCs and MFs in mice fed a LFD; analogous cells in mice fed a HFD lost these capacities, instead showing

Downloaded from https://www.pnas.org by HARVARD UNIVERSITY CABOT SCIENCE LIBRARY on February 2, 2024 from IP address 128.103.147.149.

enriched potential interactions with γδT cells (γδT), $CD8^+$ T cells, and B cells (Fig. 5*A*), suggesting a switch from a tissue-homeostatic role to a more immunomodulatory role.

To further explore potential functional roles, we focused on MF and VmSC interactions since these are two of the major populations in eVAT and have established roles in regulating tissue function and systemic metabolism. The potential interactions between eVAT Tregs and VmSCs were enriched for cytokines that inhibit adipogenesis in preadipocytes, certain of which constitute the VmSC compartment—including TNF, TGFβ, and OSM (Fig. 5*B* and *SI Appendix*, Fig. S5*A*) (29–31). In mice fed a HFD, these potential interactions were lost and replaced with putative interactions more focused on BMP7, which can promote adipogenesis and browning of white adipose tissue (31–33), and FAM3c, which is important in regulating glucose and lipid metabolism (34). The interaction analysis suggested that the eVAT Tregs enriched in lean mice, such as the two *Il1rl1*$^+$ subtypes, might be involved in inhibiting adipogenesis, a function that was potentially lost by the Tregs enriched in eVAT of obese mice, notably the *Tbx21*$^+$ subtype.

To address this notion experimentally, we first established a flow cytometry panel capable of distinguishing the three major eVAT-Treg subtypes (*SI Appendix*, Fig. S5*B*). The impact of the individual subtypes on in vitro adipogenesis was evaluated by sorting and culturing them for collection of conditioned media (CM) containing secreted mediators and then adding CM from each subtype to sorted primary preadipocytes and quantifying their propensity to engender mature adipocytes containing lipid droplets (Fig. 5*C*). The *Il1rl1*$^+$, and to a lesser degree the *Il18r1*$^+$, Treg subtypes repressed Oil-Red-O accumulation in cultured preadipocytes; on the other hand, the *Tbx21*$^+$ subtype did not have this effect (Fig. 5 *D* and *E*).

Discussion

The advent of sc technologies has highlighted the importance of heterogeneity in cell populations, including the ability to diversify tasks and improve responses to stress by "bet-hedging." The complexity of the eVAT-Treg compartment has been documented previously (14, 18), but this study has yielded several important insights related to the phenotypic and functional heterogeneity of

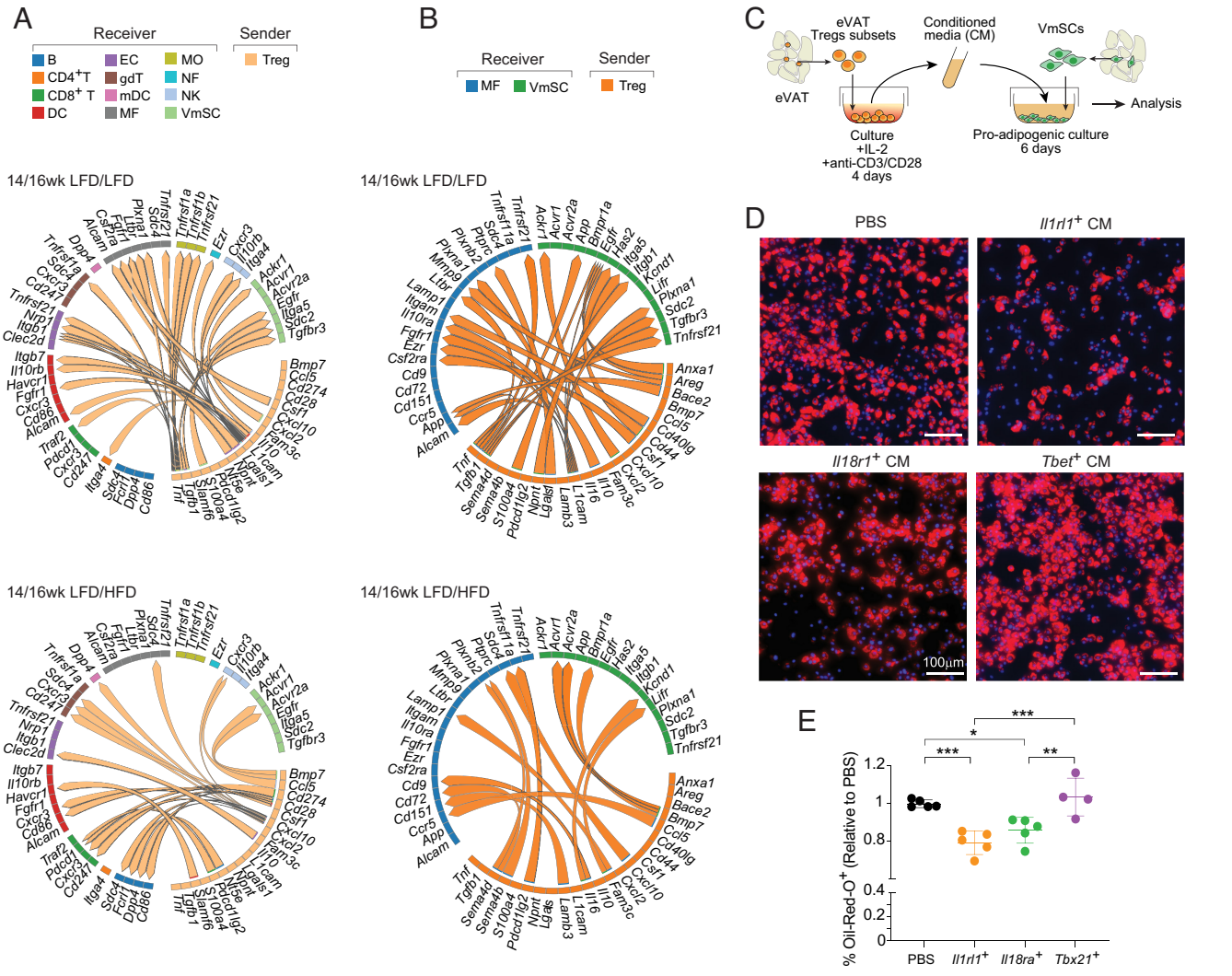

Fig. 5. Inhibition of adipogenesis by eVAT Tregs from lean vs. obese mice. (*A*) Top 50 differential ligand:receptor signals from Tregs to other cells in eVAT of lean mice challenged with HFD or not. (*B*) Top 40 differential ligand:receptor signals from Tregs to VmSCs and MFs from the same mouse groups. (*C*) Schema of in vitro adipogenesis experiments. (*D*) Immunofluorescence images of VmSCs cultured with CM from different eVAT Treg subtypes, stained for Oil-Red-O and DAPI. (*E*) Quantification of the proportion of Oil-Red-O$^+$ stained cells cultured with CM from the various eVAT-Treg subtypes. Mean ± SD, ordinary one-way ANOVA with Tukey's multiple comparisons test; *P* values: *, ≤ 0.05; **, ≤ 0.01; ***, ≤ 0.001. N = 2 independent experiments. PBS, phosphate-buffered saline; IL-2, interleukin-2; other abbreviations as per Fig. 1.

Downloaded from https://www.pnas.org by HARVARD UNIVERSITY CABOT SCIENCE LIBRARY on February 2, 2024 from IP address 128.103.147.149.

the eVAT-Treg compartment. Our data suggest a decision point as cells arrive in eVAT: to adopt either an *Il1rl1*$^+$ or a *Tbx21*$^+$ fate. The mechanism driving this decision is unclear, but one possibility is that sometime after Tregs arrive in eVAT (not necessarily immediately), they get activated by a local antigen, and then acquire a specific subtype based on the signals they received in their niche, which can vary depending on the age and diet of the mouse. In agreement with this model, the Early Activation subtype showed high expression of many T cell activation markers induced upon TCR stimulation. Some interconversion between effector subtypes also seemed to occur.

The Quiescent Treg subtype has been delineated in the Treg compartments of all nonlymphoid tissues so far examined (35) [as well as in lymphoid organs (36)]. They are a perplexing population because they express many markers characteristic of naive T cells (37); yet they are found in tissues. In the context of eVAT, our analysis suggested that the Quiescent Treg subtype instead represented a final "resting" state after the cells had been (re-)activated within the tissue. In agreement with this idea, the clusters whose trajectories pointed to the Quiescent cluster expressed higher levels of markers of T cell activation. It is possible that the cells in the Quiescent subtype represent a memory-like or stem-like phenotype of postactivated cells that are ready to respond to future challenges in the tissue, similar to tissue-resident memory cells. Another possibility is that the Quiescent state represents an "exhausted" state since many memory-like markers are shared by "anergic" or "exhausted" cells.

An outstanding question is the role of TCR specificities in establishing the various eVAT-Treg subtypes. In addition to the niche supporting Tregs in eVAT, the antigen landscape they are experiencing can also impact their differentiation and function (36, 38). But studies on a VAT-Treg TCR transgenic mouse line indicated that, in lean mice, display of a single TCR was permissive for normal development of most eVAT-Treg subtypes (5). Our TCR specificity analysis suggested that mice fed a LFD or a HFD had distinct TCR specificities and therefore different eVAT antigenic landscapes. This difference might reflect the large increases in cellularity, adipocyte death (39), endoplasmic reticulum stress (40), and posttranslational modifications (41, 42) observed in the obese state.

That the eVAT-Treg compartment of obese mice did not appear to have a large contribution from the circulating Treg pool was unexpected because a large proportion of certain of the other types of tissue immunocytes, notably MFs, do come from the circulation in obese conditions (43), and because the eVAT-Treg compartment of obese mice did take on a more splenic flavor. Instead, our data suggested that the residual eVAT Tregs that survived the obesogenic challenges proliferated locally to complete the unfilled niche, acquiring a distinct *Tbx21*$^+$ phenotype.

Thus, eVAT Tregs have distinct gene expression profiles and functional activities in obese vis-à-vis lean mice. The possibility that TCR specificities could differentially drive these activities raises the possibility of designing therapies to induce or modulate particular eVAT-Treg subtypes to better respond to an obesogenic challenge. Identifying the antigens that induce the distinct subtypes is a difficult but exciting future direction and could prove useful in mitigating metabolic disorders in contexts of obesity.

Materials and Methods

Mice. C57BL/6J and B6.CD45.1 mice were purchased from The Jackson Laboratory (stock #000664 and #002014, respectively). *Foxp3-Gfp* (44) and *Foxp3-Thy1.1* (45) mice were obtained from V. Kuchroo (Brigham and Women's Hospital, Boston, MA) and A. Rudensky (Memorial Sloan Kettering Cancer Center, New York, NY), respectively. The Kaede transgenic line (27) was obtained from O. Kanagawa (Washington University at the time). *Pparg-Tdt* mice were generated as previously described (5). Mouse ages are indicated in each figure. LFD and HFD mice were generated by feeding with a 13% kcal fat (LabDiet 5053–PicoLab) or a 60% kcal fat (Research Diets D12492i) diet ad libitum. Mice were housed at the Harvard Center for Comparative Medicine specific pathogen free facility. All animal experiments were performed following protocols approved by the Harvard Medical School Institutional Animal Care and Use Committee.

Cell Isolation and Flow Cytometry. eVAT was excised, minced, and digested with collagenase II (Sigma Aldrich) in a 37 °C water bath with shaking. Cells were stained and acquired in an Aurora Spectral analyzer (Cytek Biosciences) for analysis or were sorted on a FACS Aria II (BD Biosciences). Further details on cell manipulation and analysis can be found in *SI Appendix*, *Materials and Methods*.

scRNA-seq and sc*Tra/b*-seq. Tregs and total SVF from eVAT of 3-5 *Foxp3-Gfp* mice were pooled, hashed by groups, and then sorted and encapsulated using the Chromium 3′ v3 platform. For joint scRNA-seq and sc*Tra/b*-seq analysis, Tregs from eVAT and spleen from individual *Foxp3-Thy1.1* mice were sorted, hashed, and encapsulated using the Chromium Single Cell 5′ v2 and V(D)J platform (10× Genomics).

Data were processed using the standard cellranger pipeline (10× Genomics). Downstream analysis was done with the scanpy python package (46). Data integration was performed with the scvi-tools package (47). RNA-velocity and CellRank analysis were done with the scvelo and cellrank packages (23, 24). *Tcra/b* analysis was performed with the scirpy package (48), and N-addition analysis was performed with the IMGT V-QUEST package (49). Cell interaction analysis was performed using the MultiNicheNet package in R (28). The joint SVF and Treg datasets were used, with Treg cells set as the sender cells. Further details relating to data analysis can be found in *SI Appendix*, *Materials and Methods*.

Adoptive Transfers. Total CD4$^+$ T cells from spleens of 12- to 15-wk-old CD45.1$^+$2$^-$ mice were isolated by magnetic bead isolation using the Dynabeads Untouched Mouse CD4 kit (Invitrogen). Twelve million cells were transferred into CD45.1$^-$2$^+$ mice via retro-orbital injection. Six to ten weeks after transfer, donor-derived cells in the spleen and eVAT of host mice were analyzed by flow cytometry.

Kaede Experiments. Kaede mice were anesthetized with ketamine:xylazine (10 mg/kg:2 mg/kg, i.p), the fur on their neck was shaved, and both CLNs were photoconverted transcutaneously for 5 min with a 405-nm violet laser (<=5 mW). Photoconverted cells from the CLNs, ILNs, spleen, and eVAT were analyzed 24 h later.

In Vitro Adipogenesis Assays. To generate Treg-subtype CM, we sorted 2,000 to 3,000 cells of each of the various subtypes from eVAT of 18- to 20-wk-old *Foxp3-Gfp* mice and cultured them with IL-2 and CD3/CD28 beads, collecting supernatant every 2 d for 4 d.

Sorted VmSCs (CD45$^-$CD31$^-$PDGFRa$^+$Sca-1$^+$Thy1$^+$ PPARγ$^+$) from 12-wk-old *Pparg-Tdt* mice were cultured under proadipogenic conditions for 6 d; then, cells were fixed and stained for Oil-Red-O (Sigma) and DAPI. Cells were imaged using a Nikon Ti inverted microscope and analyzed using the FIJI software. Additional details on the culturing conditions can be found in *SI Appendix*, *Materials and Methods*.

Data, Materials, and Software Availability. All raw and processed scRNA-seq and sc*Tra/b*-seq data have been deposited in the National Center for Biotechnology Information Gene Expression Omnibus (GEO Accession No.: GSE248440) (50). A table of all identified TCRs can be found in Dataset S1. All other data are included in the manuscript and/or supporting information.

ACKNOWLEDGMENTS. We thank Dr. A. Ortiz-Lopez, K. Hattori, C. Araneo, D. Ischui Guiterrez, M. Sleeper, I. Magill, A. Baysoy, B. Vijarykumar, M. Marin-Rodero, Dr. T. Jayewickreme, and Dr. S. Galvan-Peña for experimental help and Drs. V. Kuchroo and A. Rudensky for mouse lines. Cell sorting was done at the Harvard Medical School Immunology Flow Cytometry Facility. This work was supported by grants to D.M. from the NIH (5R01 DK092541 and 1RC2 DK116691) and the JPB Foundation.

Downloaded from https://www.pnas.org by HARVARD UNIVERSITY CABOT SCIENCE LIBRARY on February 2, 2024 from IP address 128.103.147.149.

1. A. R. Muñoz-Rojas, D. Mathis, Tissue regulatory T cells: Regulatory chameleons. *Nat. Rev. Immunol.* **21**, 597–611 (2021).
2. M. Feuerer *et al.*, Lean, but not obese, fat is enriched for a unique population of regulatory T cells that affect metabolic parameters. *Nat. Med.* **15**, 930–939 (2009).
3. D. Cipolletta *et al.*, PPAR-γ is a major driver of the accumulation and phenotype of adipose tissue Treg cells. *Nature* **486**, 549–553 (2012).
4. D. Kolodin *et al.*, Antigen- and cytokine-driven accumulation of regulatory T cells in visceral adipose tissue of lean mice. *Cell Metab.* **21**, 543–557 (2015).
5. C. Li *et al.*, TCR transgenic mice reveal stepwise, multi-site acquisition of the distinctive fat-Treg phenotype. *Cell* **174**, 285–299 (2018).
6. M. Delacher *et al.*, Genome-wide DNA-methylation landscape defines specialization of regulatory T cells in tissues. *Nat. Immunol.* **18**, 1160–1172 (2017).
7. A. Vasanthakumar *et al.*, The transcriptional regulators IRF4, BATF and IL-33 orchestrate development and maintenance of adipose tissue-resident regulatory T cells. *Nat. Immunol.* **16**, 276–285 (2015).
8. C. Li *et al.*, PPARγ marks splenic precursors of multiple nonlymphoid-tissue Treg compartments. *Proc. Natl. Acad. Sci. U.S.A.* **118**, e2025197118 (2021).
9. R. G. Spallanzani *et al.*, Distinct immunocyte-promoting and adipocyte-generating stromal components coordinate adipose tissue immune and metabolic tenors. *Sci. Immunol.* **4**, eaaw3658 (2019).
10. T. Onodera *et al.*, Adipose tissue macrophages induce PPARg-high FOXP3^{+} regulatory T cells. *Sci. Rep.* **5**, 16801 (2015).
11. J. Zhong *et al.*, T-cell costimulation protects obesity-induced adipose inflammation and insulin resistance. *Diabetes* **63**, 1289–1302 (2014).
12. L. Schmidleithner *et al.*, Enzymatic activity of HPGD in Treg cells suppresses Tconv cells to maintain adipose tissue homeostasis and prevent metabolic dysfunction. *Immunity* **50**, 1232–1248 (2019).
13. C. Li *et al.*, Interferon-α-producing plasmacytoid dendritic cells drive the loss of adipose tissue regulatory T cells during obesity. *Cell Metab.* **33**, 1610–1623.e5 (2021).
14. Y. Li *et al.*, Insulin signaling establishes a developmental trajectory of adipose regulatory T cells. *Nat. Immunol.* **22**, 1175–1185 (2021).
15. Z. Zhang *et al.*, An OGT-STAT5 axis in regulatory T cells controls energy and iron metabolism. *Front. Immunol.* **13**, 874863 (2022).
16. D. Cipolletta *et al.*, Appearance and disappearance of the mRNA signature characteristic of Treg cells in visceral adipose tissue: Age, diet, and PPARγ effects. *Proc. Natl. Acad. Sci. U.S.A.* **112**, 482–487 (2015).
17. M. P. Emont *et al.*, A single-cell atlas of human and mouse white adipose tissue. *Nature* **603**, 926–933 (2022).
18. T. Xiao *et al.*, T_{regs} in visceral adipose tissue up-regulate circadian-clock expression to promote fitness and enforce a diurnal rhythm of lipolysis. *Sci. Immunol.* **7**, eabl7641 (2022).
19. F. A. Wolf *et al.*, PAGA: Graph abstraction reconciles clustering with trajectory inference through a topology preserving map of single cells. *Genome Biol.* **20**, 59 (2019).
20. S. P. Weisberg *et al.*, Obesity is associated with macrophage accumulation in adipose tissue. *J. Clin. Invest.* **112**, 1796–1808 (2003).
21. S. C. Jameson, D. Masopust, Understanding subset diversity in T cell memory. *Immunity* **48**, 214–226 (2018).
22. G. La Manno *et al.*, RNA velocity of single cells. *Nature* **560**, 494–498 (2018).
23. V. Bergen *et al.*, Generalizing RNA velocity to transient cell states through dynamical modeling. *Nat. Biotechnol.* **38**, 1408–1414 (2020).
24. M. Lange *et al.*, CellRank for directed single-cell fate mapping. *Nat. Methods* **19**, 159–170 (2022).
25. H. Huang *et al.*, Analyzing the Mycobacterium tuberculosis immune response by T-cell receptor clustering with GLIPH2 and genome-wide antigen screening. *Nat. Biotechnol.* **38**, 1194–1202 (2020).
26. M. Bogue, S. Gilfillan, C. Benoist, D. Mathis, Regulation of N-region diversity in antigen receptors through thymocyte differentiation and thymus ontogeny. *Proc. Natl. Acad. Sci. U.S.A.* **89**, 11011–11015 (1992).
27. M. Tomura *et al.*, Monitoring cellular movement in vivo with photoconvertible fluorescence protein "Kaede" transgenic mice. *Proc. Natl. Acad. Sci. U.S.A.* **105**, 10871–10876 (2008).
28. R. Browaeys *et al.*, MultiNicheNet: A flexible framework for differential cell-cell communication analysis from multi-sample multi-condition single-cell transcriptomics data. bioRxiv [Preprint] (2023). https://doi.org/10.1101/2023.06.13.544751 (Accessed 17 October 2023).
29. H. Xu, J. K. Sethi, G. S. Hotamisligil, Transmembrane tumor necrosis factor (TNF)-α inhibits adipocyte differentiation by selectively activating TNF receptor 1. *J. Biol. Chem.* **274**, 26287–26295 (1999).
30. D. Sanchez-Infantes, J. M. Stephens, Adipocyte oncostatin receptor regulates adipose tissue homeostasis and inflammation. *Front. Immunol.* **11**, 612013 (2020).
31. N. Zamani, C. W. Brown, Emerging roles for the transforming growth factor-β superfamily in regulating adiposity and energy expenditure. *Endocr. Rev* **32**, 387–403 (2011).
32. E. Casana *et al.*, BMP7 overexpression in adipose tissue induces white adipogenesis and improves insulin sensitivity in ob/ob mice. *Int. J. Obes. (Lond)* **45**, 449–460 (2021).
33. S. Qian, Y. Tang, Q. Q. Tang, Adipose tissue plasticity and the pleiotropic roles of BMP signaling. *J. Biol. Chem.* **296**, 100678 (2021).
34. X. Zhang *et al.*, FAM3 gene family: A promising therapeutical target for NAFLD and type 2 diabetes. *Metabolism* **81**, 71–82 (2018).
35. J. R. Dispirito *et al.*, Molecular diversification of regulatory T cells in nonlymphoid tissues. *Sci. Immunol.* **3**, eaat5861 (2018).
36. D. Zemmour *et al.*, Single-cell gene expression reveals a landscape of regulatory T cell phenotypes shaped by the TCR. *Nat. Immunol.* **19**, 291–301 (2018).
37. G. Escobar, D. Mangani, A. C. Anderson, T cell factor 1: A master regulator of the T cell response in disease. *Sci. Immunol.* **5**, eabb9726 (2020).
38. M. O. Li, A. Y. Rudensky, T cell receptor signalling in the control of regulatory T cell differentiation and function. *Nat. Rev. Immunol.* **16**, 220–233 (2016).
39. K. J. Strissel *et al.*, Adipocyte death, adipose tissue remodeling, and obesity complications. *Diabetes* **56**, 2910–2918 (2007).
40. G. S. Hotamisligil, Inflammation and endoplasmic reticulum stress in obesity and diabetes. *Int. J. Obes. (Lond)* **32** (suppl. 7), S52–S54 (2008).
41. A. C. Russell *et al.*, Increased central adiposity is associated with pro-inflammatory immunoglobulin G N-glycans. *Immunobiology* **224**, 110–115 (2019).
42. H. Deris *et al.*, Effects of low-calorie and different weight-maintenance diets on IgG glycome composition. *Front. Immunol.* **13**, 995186 (2022).
43. N. Cox, F. Geissmann, Macrophage ontogeny in the control of adipose tissue biology. *Curr. Opin. Immunol.* **62**, 1–8 (2020).
44. E. Bettelli *et al.*, Reciprocal developmental pathways for the generation of pathogenic effector TH17 and regulatory T cells. *Nature* **441**, 235–238 (2006).
45. A. Liston *et al.*, Differentiation of regulatory Foxp3^{+} T cells in the thymic cortex. *Proc. Natl. Acad. Sci. U.S.A.* **105**, 11903–11908 (2008).
46. F. A. Wolf, P. Angerer, F. J. Theis, SCANPY: Large-scale single-cell gene expression data analysis. *Genome Biol.* **19**, 15 (2018).
47. R. Lopez *et al.*, Deep generative modeling for single-cell transcriptomics. *Nat. Methods* **15**, 1053–1058 (2018).
48. G. Sturm *et al.*, Scirpy: A Scanpy extension for analyzing single-cell T-cell receptor-sequencing data. *Bioinformatics.* **36**, 4817–4818 (2020).
49. X. Brochet, M. P. Lefranc, V. Giudicelli, IMGT/V-QUEST: The highly customized and integrated system for IG and TR standardized V-J and V-D-J sequence analysis. *Nucleic Acids Res.* **36**, W503–W508 (2008).
50. A. R. Muñoz-Rojas, C. Benoist, D. Mathis, Adipose-tissue regulatory T cells are a consortium of subtypes that evolves with age and diet. Gene Expression Omnibus. https://www.ncbi.nlm.nih.gov/geo/query/acc.cgi?acc=GSE248440. Deposited 22 November 2023.

Downloaded from https://www.pnas.org by HARVARD UNIVERSITY CABOT SCIENCE LIBRARY on February 2, 2024 from IP address 128.103.147.149.